Journal of ELECTRONIC MATERIALS, Vol. 39, No. 9, 2010
DOI: 10.1007/s11664-010-1305-2

Modeling a Thermoelectric Generator Applied to Diesel Automotive Heat Recovery

N. ESPINOSA,[1,2,4] M. LAZARD,[3] L. AIXALA,[2] and H. SCHERRER[1]

1.—Laboratoire de Physique des Matériaux, Parc de Saurupt, Nancy, France. 2.—Renault Trucks SAS, 99, route de Lyon, Saint-Priest, France. 3.—GIP InSIC, 27, rue d'Hellieule, Saint-Dié, France. 4.—e-mail: nicolas.espinosa@volvo.com

Thermoelectric generators (TEGs) are outstanding devices for automotive waste heat recovery. Their packaging, lack of moving parts, and direct heat to electrical conversion are the main benefits. Usually, TEGs are modeled with a constant hot-source temperature. However, energy in exhaust gases is limited, thus leading to a temperature decrease as heat is recovered. Therefore thermoelectric properties change along the TEG, affecting performance. A thermoelectric generator composed of Mg_2Si/Zn_4Sb_3 for high temperatures followed by Bi_2Te_3 for low temperatures has been modeled using engineering equation solver (EES) software. The model uses the finite-difference method with a strip-fins convective heat transfer coefficient. It has been validated on a commercial module with well-known properties. The thermoelectric connection and the number of thermoelements have been addressed as well as the optimum proportion of high-temperature material for a given thermoelectric heat exchanger. TEG output power has been estimated for a typical commercial vehicle at 90°C coolant temperature.

Key words: Thermoelectric generator, modeling, EES, heat recovery, truck diesel engine

Nomenclature

Variables

B	Thermoelectric generator width, m
b_1	Height of gas channel plate, m
b_2	Height of water channel plate, m
c_p	Specific heat, J/kg/K
C_{th}	Thermal conductance, W/K
dx	Elementary length defined in Fig. 3b, m
dy	Elementary width defined in Fig. 3b, m
h	Gas heat transfer coefficient, W/m^2/K
I	Current, A
i	Point index
L	Thermoelectric generator length, m
l	Thermoelement height, m
$\dot{m}$	Mass flow rate, kg/s
n_{plate}	Number of plates within the heat exchanger
n_x	Number of thermoelement couples in the generator
n_y	Number of ranges in the generator
P_{elec}	Power recovered as described in Eq. 7, W
$P_{elec,series}$	Calculated recovered power with all thermoelements connected in series and an adapted load connected, W
Q	Heat transferred, W
$R_{elec,TE}$	Electrical resistance of a thermoelement couple, Ω
$R_{th,cont}$	Thermal contact resistance, m^2 K/W
S_h	Hot-side heat transfer surface, m^2
T	Temperature, K
U	Overall heat transfer coefficient, W/m^{2}K
ZT	Nondimensional thermoelectric figure of merit

Greek

α_{pn}	Thermoelement couple Seebeck coefficient, V/K
λ	Thermoelement thermal conductivity, W/m/K

(Received July 9, 2009; accepted May 31, 2010; published online June 23, 2010)

$\eta_{0,h}$ Overall fin efficiency
ρ Electrical resistivity, Ω m

Subscripts

cf Relating to cold fluid
cont Relating to thermal contact
hf,sup Relating to hot fluid gas
max Maximum
n Relating to n-type leg
p Relating to p-type leg

INTRODUCTION

For long-haul trucks, Diesel engines still remain the most efficient powertrain solution. Until a possible change in fuel (gas, ethanol engines) or transport (trains for cargo transport), Diesel engines will still be employed for years.

To date, regulations on Diesel engines have focused on particulate matter and NO_x (nitrogen oxide) emissions. However, recent increases in oil prices and possible CO_2 (carbon dioxide) emission regulations have encouraged the automotive industry to find solutions to improve Diesel engine efficiency.

Waste heat recovery by thermoelectrics on long-haul trucks appears to be a promising solution to improve Diesel engine efficiency. For this purpose, thermoelectric generators (TEGs) have been studied for years. Vazquez et al.[1] reviewed most past automotive projects (Porsche, Nissan, Hi-Z projects), which reported relatively low efficiencies. Saqr et al.[2] provided a basis for an efficient thermoelectric generator. Thermoelectric recovery on a truck has been implemented by Bass et al.,[3] who made a 1-kW bismuth-telluride-based electrical output generator on a 14-L Cummins NTC 275 engine. Matsubara et al.[4] made a thermoelectric stack TEG for automobiles composed of segmented legs with skutterudites followed by HZ-14 modules and achieved a 5% to 10% efficiency, depending on engine operating points. More recently, BMW/Ford, General Motors, General Electric, and Cummins companies have worked on TEG architectures with support from the US Department Of Energy.[5,6] As discussed by Hendricks et al.,[7] a thermoelectric generator should be studied as an integrated solution. The reason is that thermoelectric material properties and heat exchanger performance are closely linked.

In this paper, a study and an optimization of a simple thermoelectric architecture composed of Mg_2Si/Zn_4Sb_3 followed by bismuth telluride materials along a given thermoelectric heat exchanger are reported. Other architectures exist, such as the high-density segmented architecture recently modeled by Crane et al.[8]

A thermoelectric model based on the finite-difference method implemented in engineering equation solver software is used to investigate the ideal proportion of high-temperature material required. The numbers of thermoelements and electrical connections are addressed as well. Relevant engine operating points on a typical truck duty cycle are used as inputs in calculations to match actual engine conditions.

METHODS

Reasoning

Heat Recovery for Long-Haul Trucks

The four following potential sources are recoverable by a thermoelectric generator on a long-haul truck Diesel engine:

- Coolant water (between 90°C and 110°C);
- Exhaust gases (between 250°C and 350°C, Fig. 1b);
- Exhaust gas recirculation (EGR) gases (between 400°C and 500°C, Fig. 1a);
- Charge air cooler outlet gases (CAC) (usually around 150°C).

Exergy calculations show that the most energy can be extracted from exhaust gases. Despite the lower exhaust gas temperature (due to temperature loss in the turbocompressor) compared with the EGR temperature, exhaust gases exhibit a higher mass flow rate, which increases their exergy (available recovery).

Consequently, initial calculations presented in this paper lead to a focus on exhaust gases recovery. However, the model described herein could also be used to study an EGR thermoelectric generator.

Bulk Thermoelectric Materials

In the present study, long-haul truck exhaust temperatures (downstream after treatment systems) are usually assumed to be between 250°C and 350°C (Fig. 1). A high-pressure EGR system is considered. A TEG should not impact on the exhaust after-treatment system (EATS), which is why an end exhaust line location is proposed.

A realistic coolant temperature range is 50°C to 100°C (depending on the cooling system chosen for the TEG), namely an additional radiator or low-temperature radiator could be used to provide cooling water at 50°C. Excluding inherent losses due to imperfect thermal contact and convective resistance, a thermoelectric leg could operate between 50°C and 350°C in the generator.

In this temperature range, Bi_2Te_3 (ZT_{max} = 0.7 at 100°C) and $(Bi,Sb)_2Te_3$ (ZT_{max} = 1 at 100°C), respectively, for n- and p-type, are well-known efficient bulk materials. They have already been proposed for automotive thermoelectric generators.[3,5]

For the higher temperature range (above 220°C), bismuth telluride deteriorates. As a result, other materials should be employed. n-PbTe (ZT_{max} = 1 at 300°C) and p-PbTe (ZT_{max} = 0.7 at 420°C) are

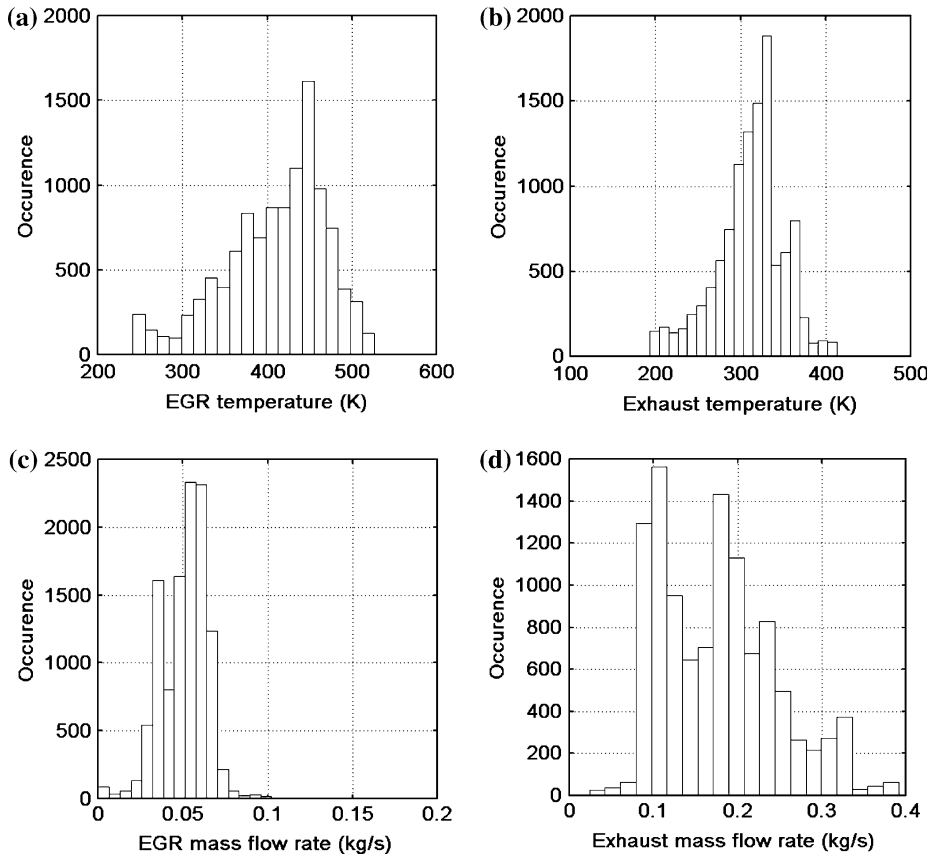

Fig. 1. Mass flow and temperature distribution of a 30-T truck equipped with a 11-L 385-hp US07 Diesel engine along a reduced Paris–Lille cycle (representative client cycle), October 2008: (a) EGR temperature distribution and (b) exhaust gases (downstream after-treatment systems) temperature distribution, (c) EGR mass flow distribution, and (d) exhaust mass flow distribution.

adequate for this higher temperature range. Other materials such as LAST have good ZT values (n-PbSbAgTe, ZT_{max} = 1.5 at 480°C, p-PbSbSnTeAg, ZT_{max} = 1.2 at 430°C).

Bulk skuterrudite materials have shown promising results[9] (n-$In_xCe_yCo_4Sb_{12}$ ZT = 1.6 at 330°C), but are still in the laboratory development phase. Despite relatively good performance, the lead contained in this material is not acceptable for most automotive companies due to environmental issues. Therefore, lead-based thermoelectric materials such as PbTe have not been selected in this study. Instead, another material couple has been used, namely n-type Mg_2SiSn and p-type Zn_4Sb_3 (for Zn_4Sb_3: ZT_{max} = 1.3 at 400°C, ZT = 1.1 at 300°C; for Mg_2SiSn: ZT_{max} = 1.1 at 370°C), which shows relatively good efficiency and could also be manufactured.

Other materials mentioned above, such as clathrates and silicon germanium, are of less interest, as their temperature ranges do not match the the exhaust temperature range (Fig. 1).

More recently, improved materials such as nano-inclusion materials, have been reported but are not used in this study as they are too far from industrialization. A long-haul truck should endure 1,000,000 km without major failure. As a consequence, only mature, bulk materials are considered in these calculations.

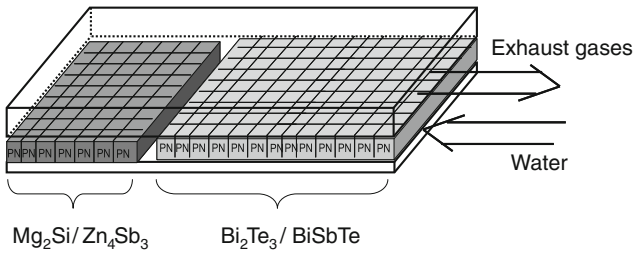

Fig. 2. Schematic view of the modeled architecture.

TEG Material Architecture

The model simulates a direct gas to liquid heat exchanger. To simplify the TEG, an indirect transfer heat exchanger (oil medium, for example) was not considered.

Two thermoelectric material types located along the heat exchanger (Fig. 2) compose the thermoelectric architecture. The high-temperature (HT) material portion (Mg_2Si/Zn_4Sb_3) and low-temperature (LT) portion (Bi_2Te_3) are then studied in the "Results and Discussion" section.

By matching the exhaust gas temperature decrease along the heat exchanger, this architecture enables the heat exchanger performance to be optimized compared with a single-material TEG. On the other hand, the cold side exhibits a low temperature change due to the high specific heat of water compared with the gases.[10,11]

Other optimizations are possible, such as cascading or segmenting thermoelements across the generator, however these architectures become more complex and fragile. Therefore, the architecture presented herein has been found as a good compromise.

TEG MODELING

Description of the Thermoelectric Generator and Basic Assumptions

The thermoelectric generator dimensions are based on an existing air/water charge air cooler geometry composed of five plates with strip fins (one unitary plate is shown in Fig. 3b). Such heat exchangers are EGR heat exchangers, designed to be compact and very efficient without major pressure drops. The base thermoelectric generator geometry is based on this charge air cooler, namely 50 cm long by 31 cm wide and 10 cm high. The size of all thermoelements is 5 mm high by 6.24 mm wide and 6.24 mm long (values close to the Hi-Z module thermoelement geometry[12]). Each gas channel has fins to decrease convective thermal resistance. Fin geometry characteristics, gas heat transfer, and pressure drop are directly known thanks to a function computed in EES (different fin geometries already exist in the program). Here, the fin geometry used is referenced sf_plate-fin_s14s-111 and characterized by a low pressure drop for high heat transferred.

Basic assumptions used in the model are summarized next. Thermoelectric properties are supposed constant in the leg but vary along the heat exchanger between legs. The Thomson effect is neglected despite the high temperature gradient. Some calculations based on Lazard et al.'s work[13] were made on a leg and showed that the temperature gradient within a leg was not modified if the current applied is not large. In our case, this current is sufficiently small. Electrical and thermal contact

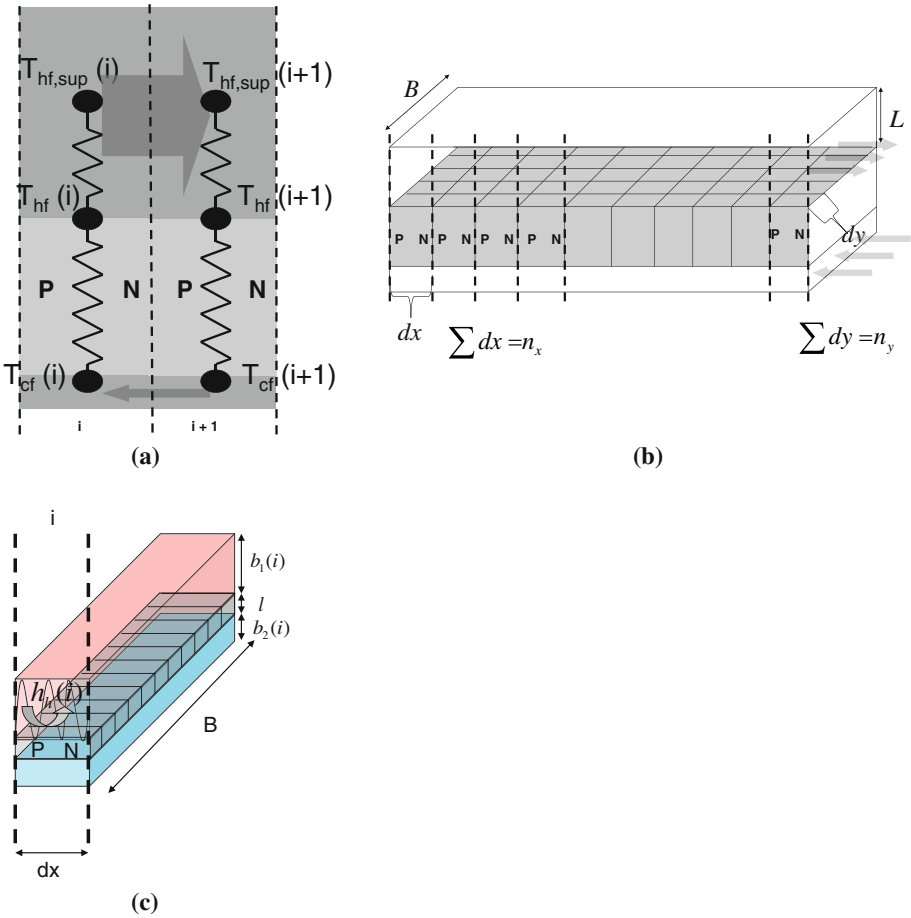

Fig. 3. Schematic of the computed EES model: (a) finite-difference scheme of the model across the thermoelement couples, (b) thermoelement layer layout including the n_x (number of couples along the heat exchanger) and n_y (number of lines of thermoelements) parameters, and (c) representation of a TEG elementary portion with variables used to calculate the overall heat transfer.

resistances are neglected (the effect of thermal contact resistance for the presented architecture is studied in the "Results and Discussion" section). The cold-side convective thermal resistance is neglected, since a high flow rate is assumed to be available, which decreases the water temperature gradient along the heat exchanger. The heat transfer coefficient used corresponds to a cross-flow compact heat exchanger, whereas finite-difference calculations are done for a pure counter-flow heat exchanger. No space is considered between thermoelements. In other words, no air (or material) is present between the thermoelectric legs. Radiative heat transfer between legs is neglected. Thermal losses (radiative and convective) to ambient are neglected. Heat transfer occurring by conduction along the heat exchanger is also neglected. The resistance of electrical connections was not taken into account.

Engineering Equation Solver Model

The basic thermoelectric model is based on a finite-difference scheme (Fig. 3a) computed using engineering equation solver (EES) software. This model is mostly inspired by that proposed by Crane,[14] adapted for exhaust gas recovery. Each heat exchange zone contains a thermoelement couple instead of a series of thermoelements as in the works by Crane[14] and Smith.[15]

TEG length is described by the number n_x of thermoelement couples placed side by side. n_y is the number of thermoelement rows in the TEG (Fig. 3b). These two parameters are adjusted to respect the heat exchanger plate dimensions specified in the "Description of the Thermoelectric Generator and Basic Assumptions" section.

$$\begin{aligned}&\dot{m}_{\mathrm{hf,sup}}c_{\mathrm{phf}}(T_{\mathrm{hf,sup}}(i)-T_{\mathrm{hf,sup}}(i+1))\\&\quad=\eta_{0,\mathrm{h}}(i)h(i)S_{\mathrm{h}}(i)(T_{\mathrm{hf,sup}}(i)-T_{\mathrm{hf}}(i)),\end{aligned}\tag{1}$$

$$\begin{aligned}&\eta_{0,\mathrm{h}}(i)h(i)S_{\mathrm{h}}(i)\left(T_{\mathrm{hf,sup}}(i)-T_{\mathrm{hf}}(i)\right)\\&=n_y\left[\begin{array}{r}C_{\mathrm{th}}(i)(T_{\mathrm{hf}}(i)-T_{\mathrm{cf}}(i))+\alpha_{\mathrm{pn}}(i)(T_{\mathrm{hf}}(i)+273)I\\-0.5I^2R_{\mathrm{elec,TE}}(i).\end{array}\right],\end{aligned}\tag{2}$$

$$\begin{aligned}&n_y\left[\begin{array}{r}C_{\mathrm{th}}(i)(T_{\mathrm{hf}}(i)-T_{\mathrm{cf}}(i))+\alpha_{\mathrm{pn}}(i)(T_{\mathrm{cf}}(i)+273)I\\+0.5I^2R_{\mathrm{elec,TE}}(i)\end{array}\right]\\&\quad=\dot{m}_{\mathrm{cf}}c_{\mathrm{pcf}}(T_{\mathrm{cf}}(i)-T_{\mathrm{cf}}(i+1)).\end{aligned}\tag{3}$$

The basic equations of the model (Eqs. 1, 2, 3) describe thermal balance for each range n_x along the exchanger (Fig. 3a).

Hot-side convective heat transfer is modeled by neglecting wall and cold-side thermal resistance. Overall heat transfer is given by Eq. 4. Heat transfer at the hot-side surface is given by $\gamma(i)$, the ratio between the heat transfer surface and volume (see Eq. 6).

Heat transfer and pressure losses for each segment $h(i)$ are described by two functions incorporated in EES, based on empirical correlations from Kays and London.[16] Necessary inputs are given in Fig. 3c. A cross-flow heat transfer coefficient is given as output as well as core pressure drops. Abrupt contraction and expansion pressure losses are not given by those functions. They are usually neglected when compared with core pressure losses.[16] This implies that care must be taken when the core section becomes large compared with the inlet section (as for the influence of the n_y variation described in the "Results and Discussion" section).

$$\frac{1}{U_{\mathrm{h}}}=\frac{1}{\eta_{0,\mathrm{h}}h}.\tag{4}$$

Energy balance is expressed in Eq. 5.

$$Q_{\mathrm{h}}(i)=U_{\mathrm{h}}(i)S_{\mathrm{h}}(i)(T_{\mathrm{hf,sup}}(i)-T_{\mathrm{hf}}(i)),\tag{5}$$

$$\gamma(i)=\frac{S_{\mathrm{h}}(i)}{(b_1(i)+b_2(i)+l)B\mathrm{d}x}.\tag{6}$$

All thermoelements run in standalone mode; in other words, the overall power calculated in the "Results and Discussion" section is given by Eq. 7.

$$P_{\mathrm{elec}}=n_{\mathrm{plate}}n_y\sum_{i=1}^{n_x}\frac{\left[\alpha_{\mathrm{pn}}(i)(T_{\mathrm{hf}}(i)-T_{\mathrm{cf}}(i))\right]^2}{4R_{\mathrm{elec,TE}}(i)},\tag{7}$$

with

$$R_{\mathrm{elec,TE}}(i)=\frac{(\rho_{\mathrm{p}}(i)+\rho_{\mathrm{n}}(i))l}{\frac{\mathrm{d}x}{2}\mathrm{d}y}.$$

Each thermoelement couple is considered to be connected to a matched load to maximize the transferred power. The electrical power P_{elec} is then given by the sum on all rows of all plates (Eq. 7). Hence, the influence of electrical connection will not be considered (see the "Influence of n_x" section).

Thermoelectric properties α, ρ, and λ are computed in the program as polynomial functions.

The model is run again to study the high-temperature part by changing the appropriate polynomial material thermoelectric properties. An optimized bismuth telluride material with better performance at higher temperature is used in these calculations.

Model Validation

Heat Exchanger Model Validation

The heat exchanger was validated against experimental data available for an air/water charge air cooler used for a prototype truck engine. Power transferred and pressure losses are known. To compare the model results with experimental testing of the heat exchanger only, the thermal

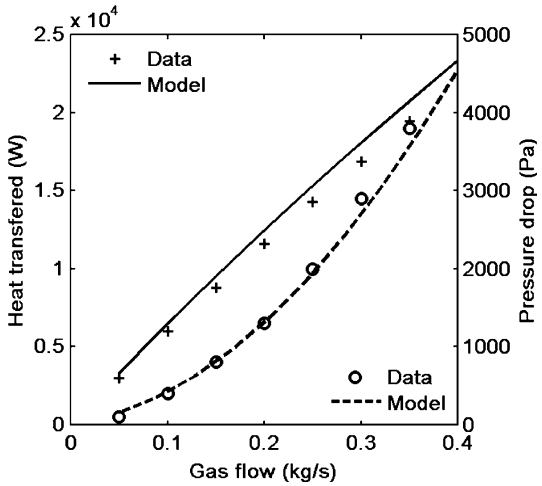

Fig. 4. Heat transferred and pressure drop model validation against charge air cooler data to validate the pressure drop part of the model.

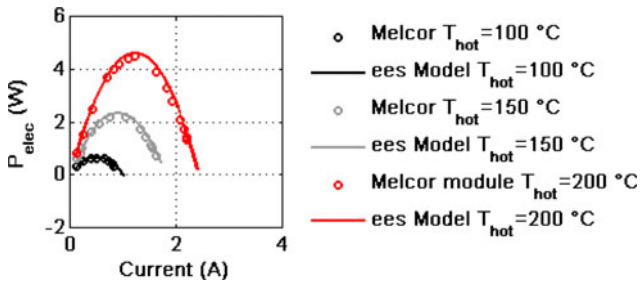

Fig. 5. Validation of the EES thermoelectric model with HT6-12-40 Melcor module characteristics; cold-side temperature is 50°C.

resistance of the TEG was reduced to zero in the model, and the results were compared with measured values for the heat exchanger. With the same fin geometry, heat transferred and pressure losses within the heat exchanger correctly matched experimental values. The pressure loss function used in EES seems to be correct regarding experimental results (Fig. 4). The heat transfer coefficient cannot be validated since no other data are available.

Thermoelectric Model Validation

The thermoelectric part of the model (from $T_{\mathrm{hf}}(i)$ to $T_{\mathrm{cf}}(i)$) was validated against properties of two well-known commercial generator modules (Hi-Z 20[12] and Melcor HT6-12-4.0[17]). In this validation, standard commercial bismuth telluride material properties were used.[18] Leg heights of 5 mm and 1.5 mm, respectively, were used in EES for the Hi-Z 20 and HT6-12-40 modules. The number of thermoelements was adjusted by varying n_x and n_y. Figure 5 shows that the electrical power computed using the EES model $P_{\mathrm{elec,series}}$ fits well with the experimental output power for the HT6-12-40 module for various hot-source temperatures and currents.

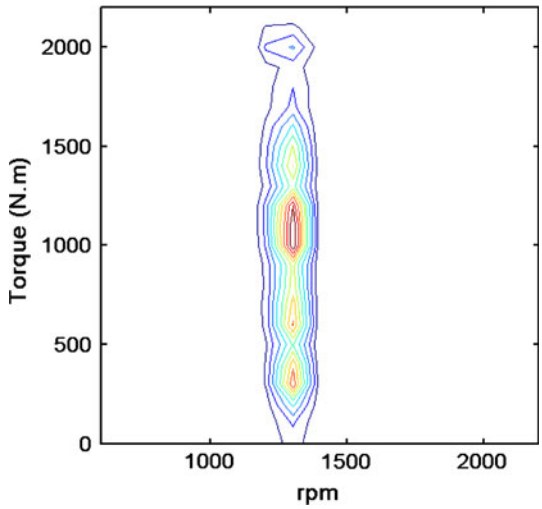

Fig. 6. Engine operating point occurrence on a Paris–Lille cycle for an 11-L 385-hp 30-T US07 engine.

An important assumption is that the properties in each discretized zone are considered at constant temperature $\frac{T_{\mathrm{hf}}(i)+T_{\mathrm{cf}}(i)}{2}$. Basic calculations on one leg have shown a small influence of thermoelectric leg discretization on output power results. The discretization consists in applying the model presented in the "Engineering Equation Solver Model" section, assuming constant thermoelectric properties on a small part of the leg. Results showed that consideration of a nondiscretized Mg_2Si leg led to a 5% overestimation compared with a discretized leg (15 parts) for a 200°C temperature difference at 10 A. Furthermore, this small influence was confirmed by the good match between experimental results and a model (using constant thermoelectric properties within the leg) for bismuth telluride modules.[15]

RESULTS AND DISCUSSION

Relevant Engine Operating Points

For a true drive cycle analysis, a transient model is required, taking into account the thermal masses of the system. This problem can be simplified by taking relevant engine operating points according to their occurrence within a classical cycle done by long-haul trucks (Paris–Lille road cycle). Four engine operating points are determined (Fig. 6) with their weighting factors (Fig. 7) for the overall cycle. Exhaust mass flow rate and temperature corresponding to each identified engine operating point are used in the calculations (Table I).

Influence of Number of Thermoelements

Influence of n_x

The number of thermoelements along the heat exchanger was varied for fixed width to investigate the impact on TEG performance.

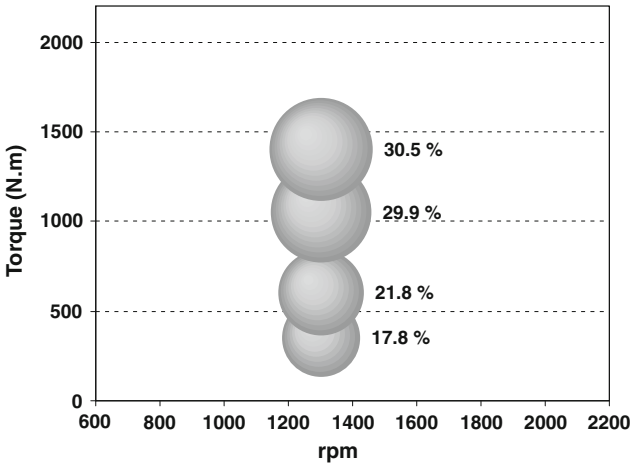

Fig. 7. Representative engine operating points and associated weighting factors on a Paris–Lille cycle for an 11-L 385-hp 30-T US07 engine.

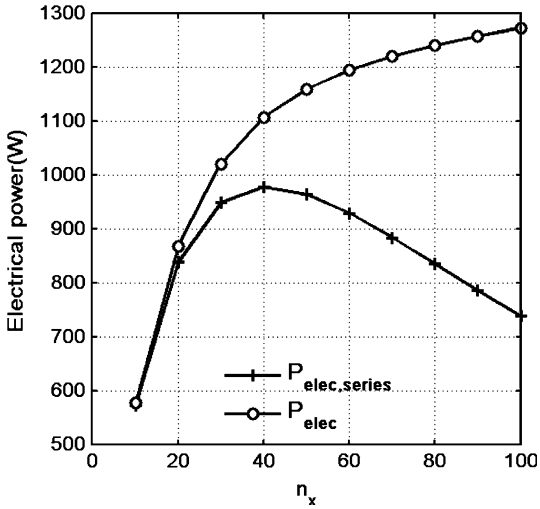

Fig. 8. Influence of number of thermoelements along the TEG on power produced, $P_{elec,series}$, with all thermoelements connected in series to a global adapted resistance and, P_{elec}, with each thermoelement connected to its dedicated adapted load; each standalone power is summarized. n_y = 50, characteristic engine operating point 3.

The base heat exchanger is 50 cm long by 31 cm wide (geometry used in the "High-Temperature/Low-Temperature Proportion Study" section).

Mg_2Si/Zn_4Sb_3 materials are used in this virtual TEG. When the TEG length (n_x) is increased, more power can be extracted, up to 1200 W for n_x = 40 against 900 W for n_x = 20 (Fig. 8). The relation is not linear, as temperature differences within the heat exchanger decrease and lead to lower thermoelement power. As a result, the power calculated by Eq. 4 tends to an asymptotic value.

When all thermoelements are connected in series, the conclusions are rather different. An optimum TEG length (or number of thermoelements) exists, giving maximum output power $P_{elec,series}$ (Fig. 8). This effect has already been reported by Mori et al.,[19] who found an optimum number of thermoelements within a TEG. Few details are given concerning internal thermoelement connection, but connection in series has been assumed. This optimum is explained as a trade-off between electromotive force and internal resistance. The latter connection configuration is not realistic practically, as failure of one thermoelement could disconnect all thermoelements.

At the opposite extreme, each thermoelement power can be connected separately with its adapted load. Omitting wiring losses, the calculated power P_{elec} is obtained (Eq. 7) without an optimum value. As a conclusion, electrical connections can influence the heat exchanger design.

In real-life applications, an intermediate power value (between P_{elec} and $P_{elec,series}$) is expected according to the connection used (mixing parallel and series connections).

Hereinafter, the influence of electrical connection is excluded by calculating P_{elec}.

Influence of n_y

n_y was varied for a fixed overall number of thermoelements. As a result, when the heat exchanger is wider, it is also shorter in length.

The width of channels in the generator tends to increase the electrical power produced (P_{elec} = 1090 W at n_y = 30 and P_{elec} = 940 at n_y = 100) and decrease the pressure drop (from 13,000 Pa at n_y = 30 to 2000 Pa at n_y = 100) (Fig. 9). However, these results have to be treated with care, because the pressure drop is taken from correlations representing core pressure drops, as discussed in the "Engineering Equation Solver Model" section.

However, as a general trend, n_y tends to increase the flow cross section. Flow speeds as well as Reynolds

Table I. Representative temperature and mass flow rate for relevant engine operating points

Engine Operating Point Reference Number	Speed (rpm)	Torque (Nm)	Weight (%)	Exhaust Temperature (°C)	Mass Flow Rate (kg/s)
1	1300	350	17.8	300	0.13
2	1300	600	21.8	312	0.14
3	1300	1050	29.9	333	0.17
4	1300	1400	30.5	330	0.22

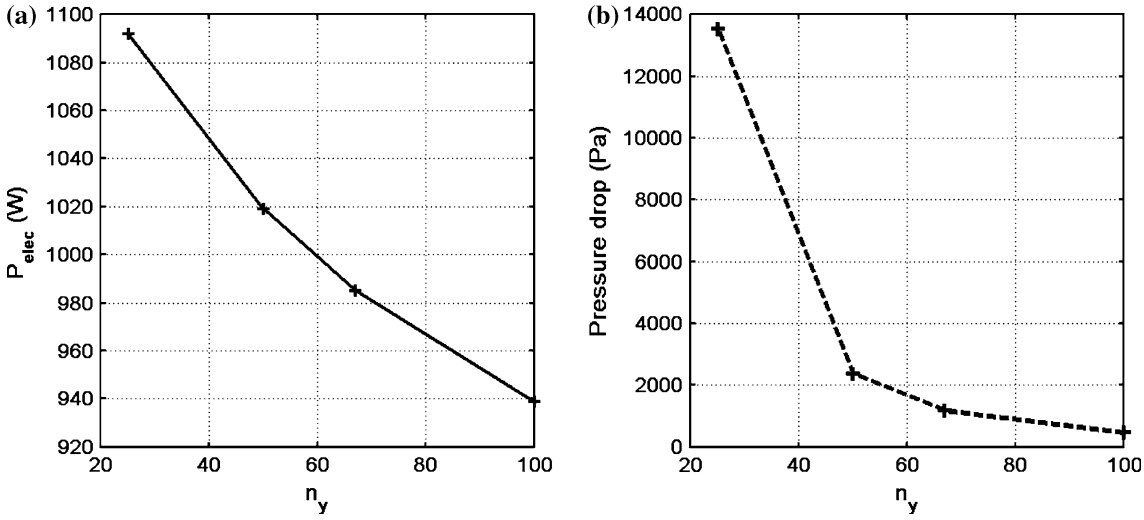

Fig. 9. Influence of n_y (TEG width) for fixed overall number of thermoelements (10,000 Mg_2Si/Zn_4Sb_3 couples) on (a) electrical power, and (b) on pressure drop.

number decrease. As a result, a lower thermal gradient ΔT is applied to the thermoelectric material due to the lower convective heat transfer. Pressure drops decrease due to the increase in flow section.

High-Temperature/Low-Temperature Proportion Study

In this section, model parameters used are n_y = 50, n_x = 40, and plate number = 5 in order to be close to validation conditions (see the "Heat Exchanger Model Validation" section).

Use of two different materials to match the temperature gradient along the thermoelectric heat exchanger slightly increases the power produced (Fig. 10). In the presented configuration (n_y = 50, five plates), for engine operating point 4 (Table I), the optimum power produced is found when the Mg_2Si/Zn_4Sb_3 portion is half of the overall material quantity. In that case, up to 1200 W can be produced, against 1050 W for a pure Mg_2Si/Zn_4Sb_3 TEG. For that particular engine operating point, the HT material proportion cannot be decreased further as this would results in too high a temperature for bismuth telluride (at 50%, the outlet zone temperature is 220°C, which is the Bi_2Te_3 critical temperature).

At engine operating points 1, 2, and 3 (Table I), the temperature and mass flow rate are lower. Hence, a smaller amount of HT material is needed to protect the low-temperature part. As a consequence, the higher-loaded engine operating point will determine the system design. For engine operating points at higher load than that of engine operating point 4, it is necessary to bypass the thermoelectric generator in order to protect the low-temperature part.

In the case of a pure Mg_2Si/Zn_4Sb_3 material generator, the heat exchanger should be bypassed when the hot-side material temperature exceeds 400°C.

A further study has been conducted to determine whether thermal contact resistance modifies the

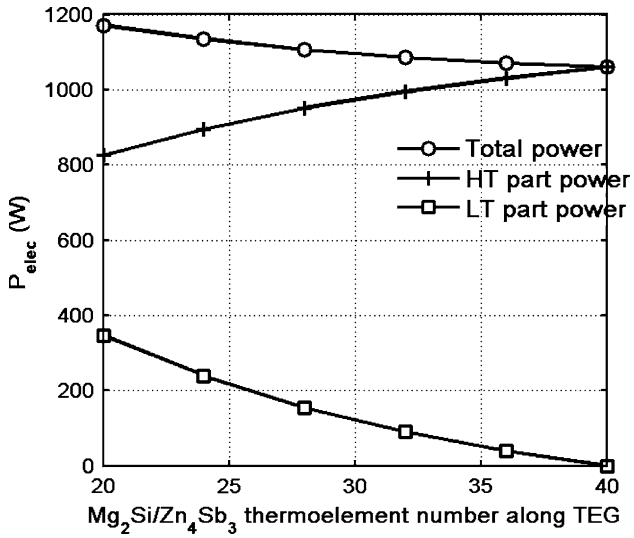

Fig. 10. Electrical power produced as a function of high-temperature material proportion along the TEG at engine operating point 1300 rpm, 1050 Nm. When n_y = 40, the heat exchanger is a full Mg_2Si/Zn_4Sb_3 TEG. ΔP is 235 Pa.

previous results. The thermal contact resistance range was chosen in a realistic range (10^{-2} m^2 K/W to 10^{-4} m^2 K/W), close to what is used in the literature.[14]

Thermal contact resistance has a major influence on the overall power produced, as reported by Hendricks et al.[7] (1000 W power produced at $R_{th,cont}$ = 10^{-4} m^2 K/W against only 800 W at $R_{th,cont}$ = 10^{-3} m^2 K/W in Fig. 11). However, the thermal contact resistance has low impact on the optimum HT material proportion in the heat exchanger. Accordingly, the power produced changes slightly with the number of Mg_2Si/Zn_4Sb_3 thermoelements along the TEG (flat curves in Fig. 11).

As a consequence, the optimum proportion of high-temperature material seems to be modified by

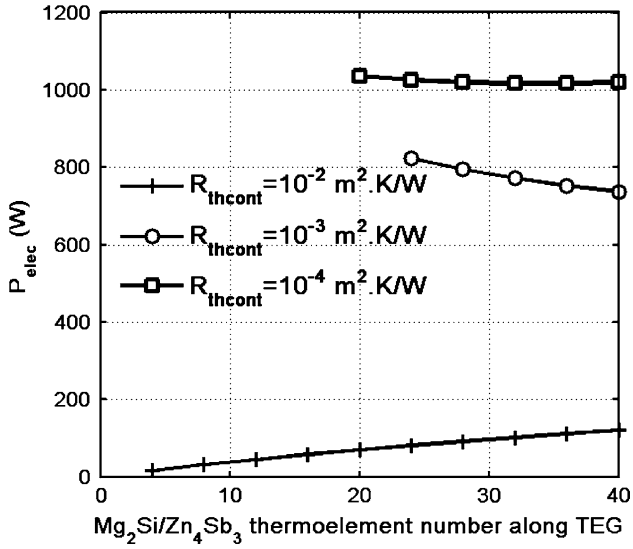

Fig. 11. Small influence of thermal contact resistance on optimum HT/LT material proportion, but strong influence on overall output power.

the exhaust and temperature conditions of the engine operating point considered, but only slightly by the thermal contact resistance.

The power has been calculated for each relevant engine operating point described in "Influence of the Thermoelements Number" and weighting factors applied to give a representative weighted cycle power. Power of 1082 W could be produced with a 50% high-temperature portion in the TEG, against 975 W for a pure Mg_2Si/Zn_4Sb_3 generator.

The power produced is higher but, regarding costs, using only Mg_2Si/Zn_4Sb_3 could be a simpler and maybe cost-effective solution.

The low exhaust gas temperature gradient explains why the bismuth telluride part of the TEG makes a low power contribution. This contribution could be increased by increasing the overall number of thermoelements or changing the height of the channels. On the other hand, this could have a negative effect on pressure drop, which needs to be limited to reduce its impact on engine back-pressure.

CONCLUSIONS

This work describes the implementation of a thermoelectric model developed using EES software, based on a finite-difference method and including hot-side convective heat transfer.

According to the electrical connection architecture used, an optimum power exists and depends on the number of thermoelements in the device.

The width of the heat exchanger modifies the convective heat transfer coefficient, which has a negative effect on the thermal difference ΔT applied to the thermoelectric material.

A generator based on two thermoelectric materials, Mg_2Si/Zn_4Sb_3 and $Bi_2Te_3/(BiSb)_2Te_3$, was simulated. For given architecture (fins, width, length, height, and plate number fixed) the optimum proportion of the two thermoelectric materials was found for a real truck duty cycle. The optimum proportion was found to be highly dependent on the engine operating point considered (temperature and gas mass flow rate) as well as the heat exchanger architecture. A bypass will be necessary to protect low temperature materials when the amount of high temperature material is not sufficient to decrease the gas temperature (low temperature materials should not exceed 250°C at the hot side).

The high-temperature material proportion does not depend on the hot thermal contact resistance. On the other hand, the thermal contact resistance has a strong influence on power results, as already reported in the literature.

Various parameters of the TEG influence its maximum power output (connection, material proportion, and size). Further studies and experiments are necessary to confirm these model results as well as to combine them to identify the most appropriate TEG for long-haul trucks. Such studies could include the effect of back-pressure on the internal combustion engine, the effect of contact resistance, the weight, and the load on the cooling system.

ACKNOWLEDGEMENT

The authors would like to thank B. Lombard for reviewing and his support.

REFERENCES

1. J. Vazquez, M.A. Sanz-Bobi, R. Palacios, and A. Arenas, *Proceedings of the 7th European Workshops on Thermoelectrics*, paper 17 # (Pamplona, 2002).
2. K.M. Saqr, M.K. Mansour, and M.N. Musa, *Int. J. Automot. Technol.* 9, 155 (2008).
3. J.C. Bass, N.B. Elsner, and F.A. Leavitt, *Proceedings of the 13th International Conference on Thermoelectrics*, AIP (Kansas City, 1994).
4. K. Matsubara, *Proceedings of the 21st International Conference on Thermoelectrics*, IEEE (2002), p. 418.
5. J. Lagrandeur, *2009 Hydrogen Program and Vehicle Technologies Program Annual Merit Review* (2009).
6. H. Shock, *2009 Hydrogen Program and Vehicle Technologies Program Annual Merit Review* (2009).
7. T.J. Hendricks and J.A. Lustbader, *Proceedings of the 21st International Conference on Thermoelectrics*, IEEE (2002), p. 381.
8. D.T. Crane, D. Kossakovski, and L.E. Bell, *J. Electron. Mater.* 38, 1382 (2009).
9. T.J. Hendricks and M. Subramanian, *Office of Vehicle Technologies 2009 Annual Merit Review* (2009).
10. H. Peter, J. de Bock, and V. Novak, *Proceedings of the Itherm Conference*, IEEE (2008), p. 1276.
11. H. Peter, J. de Bock, and V. Novak. *Proceedings of the 2nd Energy Nanotechnology International Conference*, ASME (2007), pp. 1–7.
12. Hi-Z Technology, Inc. HZ-20 thermoelectric module [on line]. Available at http://www.hi-z.com/hz20.php (2008).
13. M. Lazard, G. Fraisse, C. Goupil, and H. Scherrer, *Proceedings of the 6th European Conference on Thermoelectrics* (2008), pp. 2–15..

14. D.T. Crane (PhD Dissertation, University of Maryland, 2003).
15. K.D. Smith (Master Dissertation, Rochester Institute of Technology, 2009).
16. W.M. Kays and A.L. London, *Compact Heat Exchangers*, 3rd ed. (New York: McGraw-Hill, 1984).
17. Aztech software, Melcor, v2B (1996).
18. C.M. Jaworski (Master Dissertation, Ohio State University, 2007).
19. M. Mori, T. Yamagami, N. Oda, M. Hattori, M. Sorazawa, and T. Haraguchi, SAE, 2009-01-170 (2009).